
Article:
Liu, L. and Aitken, J.M. (2023) HFNet-SLAM: an accurate and real-time monocular SLAM system with deep features. Sensors, 23 (4). 2113.

https://doi.org/10.3390/s23042113

---

sensors

MDPI

Article

HFNet-SLAM: An Accurate and Real-Time Monocular SLAM System with Deep Features

Liming Liu and Jonathan M. Aitken *

Department of Automatic Control and Systems Engineering, The University of Sheffield, Sheffield S10 2TN, UK
* Correspondence: jonathan.aitken@sheffield.ac.uk

Abstract: Image tracking and retrieval strategies are of vital importance in visual Simultaneous Localization and Mapping (SLAM) systems. For most state-of-the-art systems, hand-crafted features and bag-of-words (BoW) algorithms are the common solutions. Recent research reports the vulnerability of these traditional algorithms in complex environments. To replace these methods, this work proposes HFNet-SLAM, an accurate and real-time monocular SLAM system built on the ORB-SLAM3 framework incorporated with deep convolutional neural networks (CNNs). This work provides a pipeline of feature extraction, keypoint matching, and loop detection fully based on features from CNNs. The performance of this system has been validated on public datasets against other state-of-the-art algorithms. The results reveal that the HFNet-SLAM achieves the lowest errors among systems available in the literature. Notably, the HFNet-SLAM obtains an average accuracy of 2.8 cm in EuRoC dataset in pure visual configuration. Besides, it doubles the accuracy in medium and large environments in TUM-VI dataset compared with ORB-SLAM3. Furthermore, with the optimisation of TensorRT technology, the entire system can run in real-time at 50 FPS.

Keywords: simultaneous location and mapping; deep features; monocular localisation

Citation: Liu, L.; Aitken, J.M. HFNet-SLAM: An Accurate and Real-Time Monocular SLAM System with Deep Features. *Sensors* **2023**, *23*, 2113. https://doi.org/10.3390/s23042113

Academic Editors: Chee Kiat Seow, Henrik Hesse, Yanliang Zhang, Torr Polakow and Kai Wen

Received: 5 December 2022
Revised: 5 February 2023
Accepted: 6 February 2023
Published: 13 February 2023

1. Introduction

Simultaneous localization and mapping (SLAM) techniques are the foundation of robot autonomy within the wider world by enabling both map building and determining the location of a robot in a hitherto unknown environment. During the last decade, with the increasing popularity of low-cost cameras, significant development has taken place in visual-based SLAM systems.

Among visual SLAM systems, feature-based methods have produced outstanding systems with increasing robustness and accuracy, such as ORB-SLAM3 [1], VINS-Mono [2], and OKVIS [3]. Most of these systems heavily rely on two types of image features based on hand-crafted principles: local and global features. However, these features may be corrupted and affect the performance of SLAM systems by challenging factors in the real world, including sparse texture, poor image quality, and occlusion [4–6].

Local features include the points of interest called keypoints and their descriptors. Extracting and matching these features in several images can provide pose estimation information [7]. Recent development of deep convolutional neural networks (CNNs) has demonstrated strong ability in feature extraction [8]. Experiments show local features based on deep CNNs have higher repeatability and matching scores even in complex environments [9], which is superior to hand-crafted features [10]. By replacing hand-crafted features with deep ones, SLAM systems can obtain more reliable environmental information [11].

Global features, also referred to as global descriptors, provide compact representations for images. Global features are essential for loop detection in SLAM systems because they help robots identify previously visited places to mitigate the accumulated drift and build a consistent map. The bag-of-word (BoW) [12] method is the most widely used method for

extracting global features from images. However, many researchers state that CNN-based loop detection methods outperform the BoW method and provide more robustness to the variance of illumination, moving objectives, and seasonal changes [13–15].

To implement the practicability of binding both local and global deep features with a real-time SLAM system and discuss the impact, this work proposes an accurate and robust monocular visual-inertial SLAM system called HFNet-SLAM. This system is a combination and extension of the well-known ORB-SLAM3 SLAM framework [1] and a unified CNN model called HF-Net [16]. To ensure real-time performance, TensorRT technology is used to optimise the CNN model. After implementation, the performance of HFNet-SLAM has been well validated in various environments among the EuRoC and TUM-VI datasets to illustrate the accuracy and efficiency of the whole system.

2. Background Literature

2.1. Visual SLAM

There is extensive research on visual SLAM systems. Davison proposed MonoSLAM in 2003, beginning the era of monocular SLAM [17]. This algorithm uses an extended Kalman filter (EKF) to achieve real-time localization with sparse prior scene knowledge. However, this pure visual SLAM performs poorly with occlusions, motion blur, and trackable texture sparsity. To address this problem, the multi-state constraint Kalman filter (MSCKF) [18] allows the incorporation of an inertial measurement unit (IMU) with vision. MSCKF is a tightly coupled visual-inertial algorithm in which several camera poses and IMU measurements are updated and jointly optimized.

Although EKF-based SLAM systems are simple and straightforward, researchers are always striving to improve their accuracy. Keyframe-based approaches and bundle adjustment (BA) optimization [19] are used to improve the accuracy at the expense of higher computation. VINS-Mono [2] is a very robust odometry estimation system. It maintains the recent states of map points and cameras in a fixed-size sliding window and updates them by iteratively solving BA. ORB-SLAM3 [1] strengthens the ability to reuse a map to build a co-visibility graph. It uses short-term, mid-term, and long-term data association in local visual-inertial BA and an effective IMU initialization technique to achieve remarkable accuracy in indoor environments.

The rapid development of neural networks brings considerable benefits to visual SLAM technology. Li et al. proposed a deep convolutional neural network (CNN) to accurately estimate depth information for mapping from two consecutive monocular images [20]. DeepVO [21] introduced an end-to-end recurrent CNN (RCNN) for pose estimation. This algorithm directly inferred poses from an RGB-D stream without the pipeline of traditional visual odometry (VO), like feature matching, pose optimisation, and so on. DeepSLAM [22] extended the previous ideals and employed three different types of CNNs for tracking, mapping, and loop closing. RDS-SLAM [23] incorporated a deep learning application for semantic segmentation into a SLAM framework to reduce the negative impact of moving objects on accuracy. Although some deep SLAM work has achieved impressive accuracy improvements, real-time performance and the ability to transform the network for various scenarios remain challenges [24].

2.2. Visual SLAM with Deep Features

2.2.1. Local Features

Most of the current leading visual SLAM systems rely on matching 2-D keypoints in frames or 3-D map points according to the similarity of their descriptors. Hand-crafted features, including ORB [25], Shi-Tomasi [26], and BRISK [27], have been widely used for their efficiency [7]. These traditional features, however, have been shown to be inaccurate and unstable, reducing the robustness of tracking and mapping in classical localization methods [28–30]. Local features emerging from deep learning significantly outperform these traditional features. DeTone et al. introduced a self-supervised fully convolutional model called SuperPoint to compute pixel-wise features with outstanding matching abil-

ity [9]. Ono et al. designed a deep network that allows training without hand-crafted priors and produces robust features in both indoor and outdoor environments [31]. SLAM systems can get such benefits by applying deep features. The GCN-SLAM proposed the GCNv2 network to replace the ORB algorithm for extracting local features in the ORB-SLAM2 framework. The authors concluded that the GCNv2 net produced better distributed features than the hand-crafted features, which led to a better quality of tracking [32]. In addition, DF-SLAM also successfully combined learned features with traditional visual SLAM systems, demonstrating good accuracy and real-time performance [33].

2.2.2. Global Features

Global features provide an effective solution for image retrieval and place matching. The majority of modern SLAM systems rely on BoW [12] for place recognition. This method clusters local features into visual words and aggregates the presence or absence of visual words to generate the representation of an image [34]. However, significant drawbacks have been reported in recent years. Garcia-Fidalgo et al. stated that the pre-trained vocabulary in an offline step only achieves correct results in generic environments and may lead to false detection in unexplored environments [35]. Zhang et al. highlighted that the BoW descriptors merely represented the appearance of features without any geometric relationship, which thereby led to poor performance in places with similar features [36]. However, deep CNN-based approaches have shown great power in representing images. Arandjelovic et al. proposed NetVLAD, which aggregated high-level features in convolution layers to produce a global feature in a fixed-length vector [37]. Hausler et al. further extended NetVLAD to include a multi-scale fusion of features to enhance place recognition performance in challenging environments [38]. Such efforts have produced remarkable results in a variety of SLAM algorithms. Yang et al. introduced the NetVLAD model into a multi-camera visual SLAM system, and they declared that loop detection based on deep learning methods showed excellent robustness to some factors, such as rough roads, different viewpoints, and changing illumination in off-road scenarios [39]. Kuse et al. designed a loop detection model based on deep features. Their experiments showed that deep global features provided a more comprehensive description of images compared with traditional methods, leading to high recall and precision in loop detection [40].

2.2.3. Joint Local and Global Features

Although the deep features bring significant improvements, inferring multiple models for extracting local and global features can be extremely expensive for a real-time SLAM system. To solve this problem, it is natural to consider combining two types of features in a single model. Cao et al. devised a model called DELG, which unified local and global features into a single deep model to reduce the computation cost by sharing calculations [41]. Based on the same ideal, the authors of [16] used MobileNet [42] as the backbone, combining a SuperPoint encoder [9] and a NetVLAD layer [37] to output local and global features. Furthermore, they introduced a distillation training method to reduce the complexity of the model. Their model, called HF-Net, can run in real time and has outstanding performance in complex environments. Although these unified models have achieved success in the structure from motion (SFM) problem, they have not been widely accepted in the SLAM domain. DXSLAM [43] is the first step towards building such a system. It incorporated HF-Net into the framework of traditional RGB-D SLAM and proved that the introduction of unified models can improve the performance of SLAM systems with RGB-D sensors. However, the disadvantages of DXSLAM are apparent. Firstly, DXSLAM does not use the image pyramid strategy while extracting local features, producing a small number of keypoints, and corrupting the accuracy of the system in a complex environment. Secondly, this system failed to take full advantage of global features generated by HF-Net. It still relies on the BoW method for loop detection and keypoint matching. Last but not least, the evaluation results of DXSLAM are unconvincing because the authors only demonstrate the quantitative error comparison in five sequences in similar environments.

HFNet-SLAM is based on the work mentioned above. In this work, the ORB-SLAM3 framework is used as the structural backbone. HF-Net optimised by TensorRT is chosen for feature extraction because of its special design for efficiency, though its production may not be the most accurate among other similar works. To take full advantage of the deep features, HFNet-SLAM proposes effective and accurate keypoint processing and loop detection modules without the assistance of the hand-crafted features and BoW algorithm. HFNet-SLAM, in contrast to most similar works that use RGB-D sensors, is intended for monocular cameras. The work of HFNet-SLAM is more fundamental and can be further extended to stereo and RGB-D SLAM.

3. HFNet-SLAM

3.1. Overview

Figure 1 shows the main components of the proposed monocular visual-inertial SLAM system, called HFNet-SLAM. This system is built on ORB-SLAM3 [1] and thus shares plenty of the same components with it. The system starts with a tracking thread, in which the local features are tracked and IMU data are integrated to estimate the pose of the current frame. Once a frame is decided to be a keyframe by the tracking thread, further operations, including global feature extraction, keypoint triangulation, and local BA, are performed on the keyframe in the mapping thread. Based on the global features, an effective loop closure method is proposed to eliminate the accumulated drift in the loop closure thread.

Compared with ORB-SLAM3, the distinguishing feature of HFNet-SLAM is that the local features (keypoints and corresponding descriptors) and global features are extracted from a deep CNN, HF-Net, instead of the traditional ORB and BoW methods. Therefore, some parts of the system, including feature extraction, keypoint matching, and loop detection, are customized for this modification.

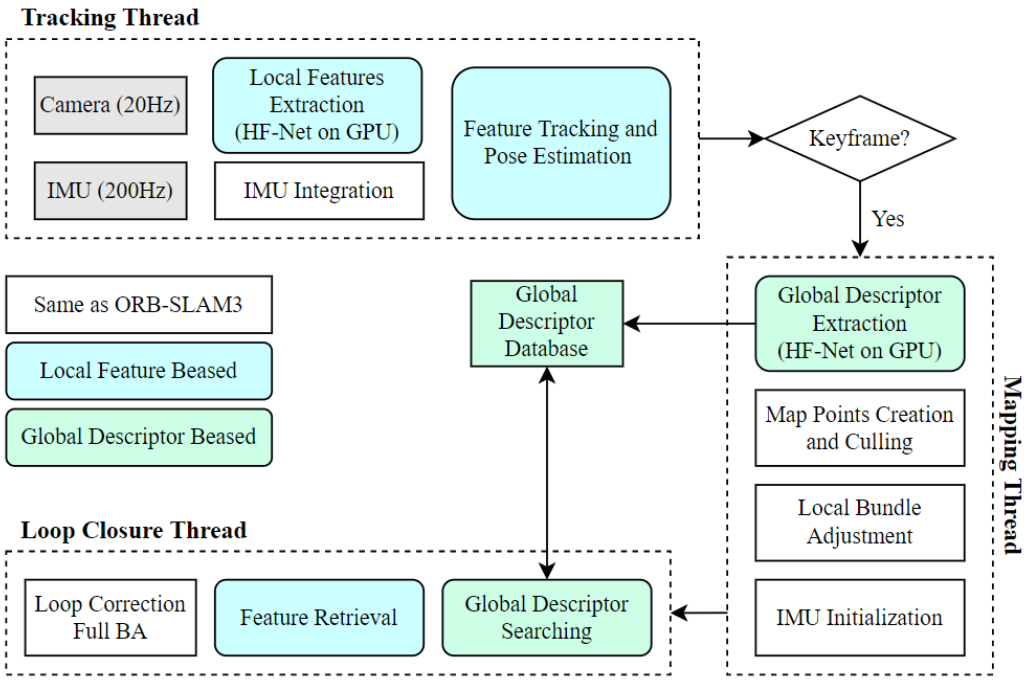

Figure 1. The main components of HFNet-SLAM framework.

3.2. Feature Extraction

The deep convolutional neural network, HF-Net [16], is used to extract local and global features from the input frames. There are two potential improvements to increase the adaptability of HF-Net in SLAM systems. Firstly, the original HF-Net model does not support the widely used image pyramid strategy in SLAM systems. Besides, the model calculates global features for every frame, which is not required by SLAM systems, causing

unnecessary calculation. Therefore, the original HF-Net is divided into two parts: the local and global parts, each running on two threads, respectively. The process of feature extraction is plotted in Figure 2.

The local part of HF-Net contains a MobileNet [42] and a SuperPoint [9] encoder. It takes an image as input and generates keypoints and corresponding descriptors, as well as the shared features for further calculation. Several local parts are deployed on the tracking thread. In this thread, the input frame is copied and iteratively scaled down to form an image pyramid. For each level in the pyramid, the scaled image passes through a local part of the model to collect the local features.

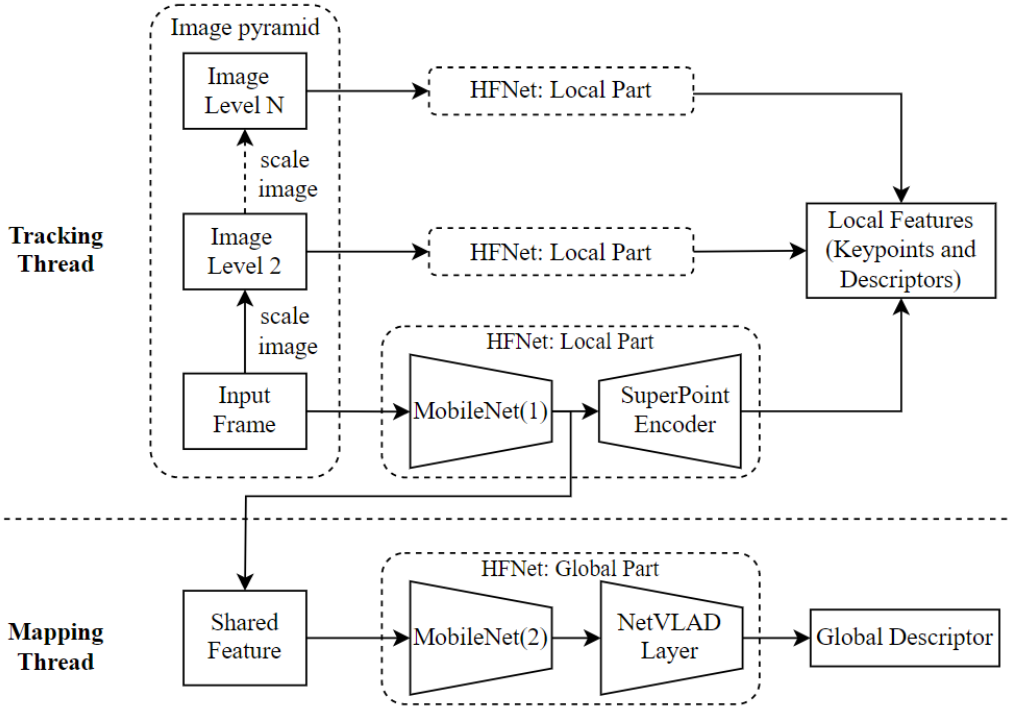

Figure 2. The feature extraction process of HFNet-SLAM.

The global part of HF-Net, consisting of another MobileNet and a NetVLAD layer [37], is employed in the mapping thread for processing keyframes. The previously calculated shared features from the tracking thread are reused to obtain the global features for the input image.

This process has several benefits. Firstly, the image pyramid enables multi-detection for the same image with different resolutions, which increases the number and scale-invariant characteristics of local features. Besides, the global features are only further calculated for keyframes. The reuse of shared features and the avoidance of unnecessary calculations effectively reduce the cost of the feature extraction process.

The original HF-Net model is implemented in TensorFlow. The performance of model prediction can be improved by the TensorRT toolkit [44]. To reduce the latency of inference, the pre-trained HF-Net model is optimized and deployed with the TensorRT engine on NVIDIA GPU devices.

3.3. Keypoint Matching

Keypoint matching strategies with good performances are essential for HFNet-SLAM. These strategies find the correspondences between keypoints in frames and maps to provide geometric constraints for pose estimation.

HFNet-SLAM has two types of matching strategies for different scenarios. 3-D–2-D matchers are used for tracking 3-D points on maps with 2-D keypoints on frames. Matchers project map points onto the image and only match keypoints nearby the projection area.

However, 2-D–2-D matchers for tracking 2-D keypoints in different frames can be extremely expensive since matchers have to match a large number of possible pairs. To bound the computation complexity, traditional systems, including ORB-SLAM3 and DXS-LAM, only match a limited number of putative matches between keypoints provided by a pre-trained BoW vocabulary tree [1,43]. In order to get rid of the dependence on the BoW algorithm, HFNet-SLAM has to use brute-force matchers on the full set of possible keypoint pairs. This unacceptable computation cost may corrupt the real-time performance.

The process of matching can benefit from vectorization technology. The descriptor of a keypoint generated by HF-Net is a vector of 256 floating numbers, denoting as $v \in \mathbb{R}^{256}$. Considering an image with a set number of keypoints, their descriptors can be concatenated to form a matrix $V = [v^1, v^2, \cdots, v^n]^T \in \mathbb{R}^{n \times 256}$, where n is the number of keypoints. HFNet-SLAM uses L_2-norm between descriptors to measure the matching score. Since the descriptor matrix is normalized, the pairwise matching score between rows of V_1 and V_2 can be simplified as:

$$score = \sqrt{V_1 V_1^T + V_2 V_2^T - 2 V_1 V_2^T} \approx \sqrt{2 - 2 V_1 V_2^T} \tag{1}$$

The matrix multiplication $V_1 V_2^T$ can be sped up by using parallel calculation and single-instruction-multiple-data (SIMD) technology on modern CPUs. Although this method cannot avoid unnecessary calculations, it greatly improves the CPU throughput to increase computational efficiency [45].

3.4. Loop Detection

Loop detection is essential for the SLAM system to eliminate the accumulated errors. Using the BoW method for loop detection is the most popular choice for recently proposed SLAM systems. However, this method has limited power to describe the whole image [36] and only obtains 50%-80% precision and recall [12]. As a result, the traditional BoW-based loop detection method tends to employ stringent verification criteria to avoid false positives that could harm the SLAM system. As Figure 3 shows, in ORB-SLAM3, loop candidates are selected through multiple factors. Such verification can improve the precision of the retrieval at the cost of reducing recall and efficiency.

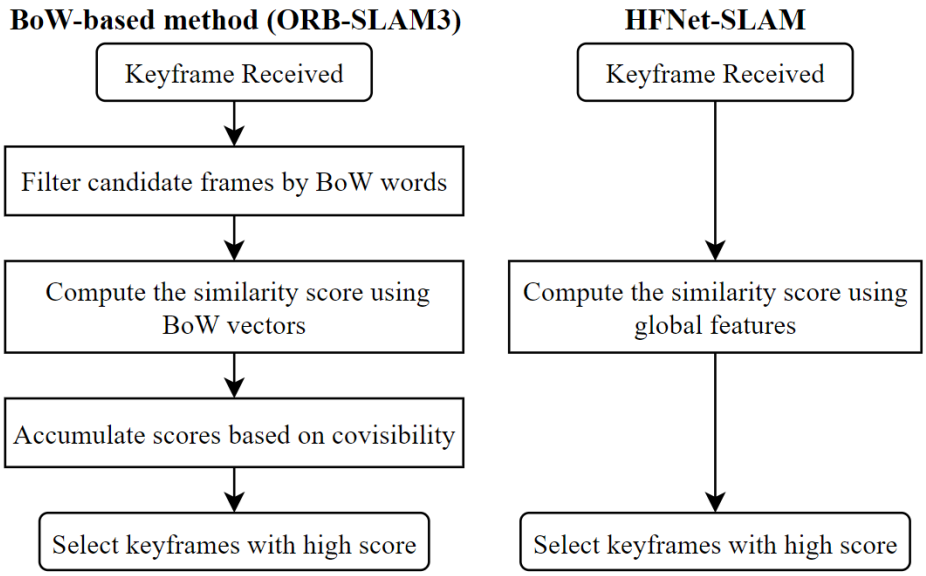

Figure 3. Plot of image retrieval modules in ORB-SLAM3 and HFNet-SLAM.

Due to the high accuracy of CNN-based global features, the proposed loop detection in HFNet-SLAM is straightforward and effective. The process begins with an image retrieval

module, as shown in Figure 3. This module calculates the similarity between images according to their global features. Several candidate images from the database are selected based on a high score with the query image. The similarity score between two global features x and y is computed by L_2-norm:

$$s(x, y) = 1 - \sqrt{\sum_{i=1}^{n} (x_i - y_i)^2} \quad (2)$$

where, x and y are the global feature vectors from two images. $n = 4096$ is the dimension of vectors. $s(x, y)$ is the similarity score of two images, and the higher the similarity, the greater the possibility of becoming a loop.

After several loop candidates are detected by image retrieval, geometric verification is used to improve the accuracy of loop closure. First, keypoint matchers are used to establish feature correspondences between the candidate frame and the query frame. For these matches, a 3-D alignment with RANSAC [46] is used for outlier rejection and transformation estimation. After geometric verification on three co-visible keyframes, this candidate frame is regarded as a genuine loop.

This deep learning-based loop detection is both accurate and effective. This improvement leads to the better performance achieved by HFNet-SLAM in contrast to ORB-SLAM3 in the TUM-VI and runtime performance experiments.

4. Results

In this section, the HFNet-SLAM system is implemented in C++, and the HF-Net model is calculated with the TensorRT C++ API for a uniform programming language and better efficiency. After implementation, the entire system is evaluated in public benchmarks against different state-of-the-art systems. Two different experiments, including SLAM experiments and runtime evaluation, are performed to evaluate the performance in terms of accuracy, stability, and computational cost.

During evaluation, the experiments of HFNet-SLAM run on an Intel Core i7-10750H CPU, at 2.6 GHz, with 16 GB memory and an NVIDIA RTX 2070 with Max-Q Design GPU, with 8 GB memory. Considering the various environmental features in test benchmarks, the number of extraction features for every input image is adjusted to get a trade-off between reducing computational cost and collecting sufficient information in a complex environment. Besides, other systems available in the literature run with their default configuration.

4.1. SLAM Experiment

In this experiment, the HFNet-SLAM and other state-of-the-art systems are performed on the EuRoC [47] and TUM-VI [48] datasets to validate the overall accuracy and robustness. For each sequence in the datasets, the poses for all frames are evaluated by different SLAM algorithms. Then, the estimated poses are aligned with the corresponding ground-truth positions using Sim(3) transformation in the pure monocular case, and using SE(3) transformation in the visual-inertial case. After that, the rms ATE (absolute trajectory error) [49] is calculated as the evaluation metric to compare the performance of various systems. For the visual-inertial case, the scale errors are also calculated using s from Sim(3) alignment.

4.1.1. Monocular SLAM on EuRoC Dataset

The EuRoC dataset is a widely used and accepted benchmark by SLAM developers. This dataset is composed of 11 sequences of small indoor environments. It provides stereo images recorded at 20 FPS, IMU measurements at 200 Hz, as well as full ground-truth data of camera motions [47]. During evaluation, only the images from the left camera are used for the monocular SLAM. HFNet-SLAM takes 752 $\times$ 480 images as inputs and extracts 675 keypoints for every image.

Figure 4 demonstrates the evaluation results of the HFNet-SLAM with monocular and monocular-inertial configurations. The obtained results are also compared with other relative state-of-the-art SLAM systems, including ORB-SLAM3 [1], DSM [50], and VINS-Mono [2].

Seq.	Monocular			Monocular Inertial				
	DSM	ORB-SLAM3	HFNet-SLAM	VINS-Mono	ORB-SLAM3		HFNet-SLAM	
	ATE	ATE	ATE	ATE	ATE	scale error	ATE	scale error
MH01	0.039	0.016	**0.015**	0.084	0.062	1.4%	**0.023**	0.3%
MH02	0.036	0.027	**0.020**	0.105	**0.037**	0.3%	0.053	0.9%
MH03	0.055	**0.028**	0.038	0.074	0.046	0.8%	**0.042**	0.6%
MH04	0.057	0.138	**0.054**	0.122	0.075	0.5%	**0.063**	0.4%
MH05	0.067	0.072	**0.042**	0.147	**0.057**	0.3%	0.069	0.7%
V101	0.095	0.033	**0.032**	0.047	0.049	2.0%	**0.044**	1.7%
V102	0.059	0.015	**0.012**	0.066	**0.015**	0.6%	**0.015**	0.7%
V103	0.076	0.033	**0.022**	0.180	0.037	2.2%	**0.036**	1.8%
V201	0.056	0.023	**0.017**	0.056	**0.042**	0.7%	0.052	0.4%
V202	0.057	0.029	**0.014**	0.090	0.021	0.4%	**0.016**	0.2%
V203	0.784	-	**0.042**	0.244	**0.027**	1.0%	0.031	0.4%
Avg	0.126	0.041*	**0.028**	0.110	0.043	0.9%	**0.040**	**0.7%**

Figure 4. Comparison results in EuRoC dataset (rms ATE in meters; scale error in %). The results of HFNet-SLAM are median of ten executions. The measurements of other systems are provided by [1]. The bold values denote the smallest errors. Asterisks mark systems that did not complete all sequences

In the monocular-inertial case, HFNet-SLAM has the most precise results among these systems, obtaining errors below 5 cm for most of the sequences. Compared with ORB-SLAM3, HFNet-SLAM can provide a more accurate scale evaluation, leading to a slight improvement in the average ATE. In this case, the estimated results by different algorithms in *V202* sequence are plotted in Figure 5a. As can be seen, plenty of regions are revisited during the tracking. HFNet-SLAM and ORB-SLAM3 use mid-term data association to reuse previous regions, leading to low trajectory errors of 2 cm, while VINS-Mono only optimises frame states over a bounded-size sliding window, which causes a considerable drift in the trajectory.

In the pure monocular case, HFNet-SLAM has an average rms ATE of 2.8 cm, which outperforms ORB-SLAM3 and more than trebles the accuracy of DSM. However, due to fast motions, HFNet-SLAM fails to track in the *V203* sequence, as illustrated in Figure 5b. Due to the reliable loop detection module, this algorithm can still re-localise itself in previously visited locations and estimate parts of the trajectory with relatively low error in each execution. Compared with the pure vision case, the inertial integration enables the system to predict the camera motions when experiencing tracking loss, boosting the robustness and stability of the system.

To conclude, the appropriate application of deep features improves the scale estimation and tracking quality of the SLAM system. Therefore, HFNet-SLAM achieves more precise results than ORB-SLAM3 in both monocular and monocular-inertial cases.

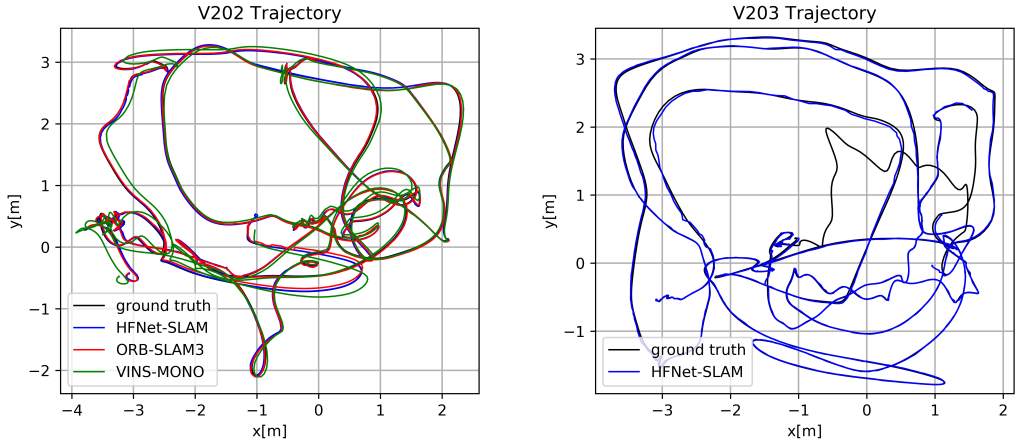

(**a**) (**b**)

Figure 5. (**a**) Estimated trajectories in *V202* sequence with monocular-inertial configuration; (**b**) Estimated trajectories in *V203* sequence with pure monocular configuration

4.1.2. Visual-Inertial SLAM on TUM-VI Dataset

The circumstances in the EuRoC dataset are small, simple, and easy to solve. Therefore, the evaluation results in this benchmark may not represent its actual performance in real robot deployments. The TUM-VI dataset is more challenging than EuRoC dataset. It not only contains small indoor environments but also records environments with more difficult factors in the real-world scene, including corridors, outdoors, moving objects, and textureless structure [48]. However, TUM-VI dataset does not provide full ground-truth data for camera motions as the information is only captured in a room at the beginning and end of the trajectory. To avoid loop closure in these scenarios, viewpoint directions are opposite and no common region can be detected. Therefore, the evaluated ATE can still represent the accumulated drift during tracking.

During the evaluation, HFNet-SLAM takes 512 $\times$ 512 images as inputs. The system extracts 850 keypoints for every image to overcome the complexity of the environment. Figure 6 compares the accuracy of HFNet-SLAM using the monocular-inertial configuration with VINS-Mono and ORB-SLAM3. As the table shows, HFNet-SLAM has the most precise results among these systems in different scenarios. Especially in medium and large environments, HFNet-SLAM outperforms other systems in most of these sequences by a wide margin.

In small indoor environments, *room* and *corridor* sequences, the environment of these sequences is similar to that of the EuRoC dataset. Due to the advantages of region-reusing ability, both the HFNet-SLAM and ORB-SLAM3 systems achieve very good results in such environments. The average errors obtained by HFNet-SLAM are only 1 cm in *room* sequences and 8 cm in *corridor* sequences, which are smaller than other systems. These results further support the previous analysis in the EuRoC dataset evaluation that the employment of deep features brings benefits to the accuracy of the system in small indoor environments.

In medium and large environments, *magistrale* and *outdoors*, the performance of HFNet-SLAM is significantly better than other systems. In half of these sequences, HFNet-SLAM is twice as accurate as ORB-SLAM3 and has more than five times the precision of VIN-Mono. These are two key reasons for the improvement.

Sequence	Mono-Inertial			Length (m)	LC
	VINS-Mono	ORB-SLAM3	HFNet-SLAM		
corridor1	0.63	0.04	**0.023**	305	Y
corridor2	0.95	**0.02**	0.048	322	Y
corridor3	1.56	0.31	**0.036**	300	Y
corridor4	0.25	**0.17**	0.227	114	
corridor5	0.77	**0.03**	0.051	270	Y
average	0.83	0.11	**0.077**	-	-
magistrale1	2.19	0.56	**0.130**	918	Y
magistrale2	3.11	0.52	**0.471**	561	Y
magistrale3	**0.40**	4.89	2.903	566	
magistrale4	5.12	**0.13**	0.184	688	Y
magistrale5	**0.85**	1.03	0.874	458	Y
magistrale6	2.29	1.30	**0.604**	771	Y
average	2.33	1.41	**0.861**	-	-
outdoors1	74.96	70.79	**42.575**	2656	
outdoors2	133.46	**14.98**	15.312	1601	
outdoors3	36.99	39.63	**12.965**	1531	
outdoors4	16.46	25.26	**14.887**	928	
outdoors5	130.63	14.87	**12.770**	1168	Y
outdoors6	133.60	16.84	**14.036**	2045	
outdoors7	21.90	7.59	**0.605**	1748	Y
outdoors8	83.36	27.88	**10.251**	986	
average	78.92	27.23	**15.425**	-	-
room1	0.07	0.01	**0.008**	146	Y
room2	0.07	0.02	**0.012**	142	Y
room3	0.11	0.04	**0.013**	135	Y
room4	0.04	**0.01**	0.016	68	Y
room5	0.20	0.02	**0.012**	131	Y
room6	0.08	0.01	**0.006**	67	Y
average	0.10	0.02	**0.011**	-	-
slides1	0.68	0.97	**0.414**	289	
slides2	0.84	1.06	**0.803**	299	
slides3	0.69	0.69	**0.611**	383	
average	0.74	0.91	**0.609**	-	-

Figure 6. Comparisonresults in TUM-VI dataset (rms ATE in meters). The results of HFNet-SLAM are median of five executions. The measurements of other systems are provided by [1]. The bold values denote the smallest errors. LC means whether the loop closure may exist.

Firstly, the proposed loop detection strategy in HFNet-SLAM is accurate and reliable. In *magistrale* and *outdoors* sequences, common regions are rare and difficult to detect. Figure 7 records the performance of loop detection modules in these sequences where loops may exist. As can be seen, compared with ORB-SLAM3, HFNet-SLAM has higher recall and tends to recognise more correct loops in complex environments during the evaluation, resulting in up to a 97% reduction in trajectory errors. This is further explained in Figure 8, which compares trajectories estimated by HFNet-SLAM and ORB-SLAM3 in the *outdoors7* sequence. In this sequence, HFNet-SLAM successfully detects three potential loop closures during the tracking, while ORB-SLAM3 fails to take advantage of all loop information and misses two of them. The missed loop detection causes error accumulation in the trajectory of ORB-SLAM3, leading to an error of more than 7 m. The novelty of loop detection explains the dramatic improvement in accuracy.

Sequence	ORB-SLAM3				HFNet-SLAM			
	LC count	ATE with LC off	ATE with LC on	ATE reduction	LC count	ATE with LC off	ATE with LC on	ATE reduction
magistrale1	1	2.05	0.56	72.7%	4	5.30	0.13	97.5%
magistrale2	1	0.72	0.52	27.9%	1	0.61	0.47	22.5%
magistrate4	0	-	0.13	-	1	1.03	0.18	82.2%
magistrale5	0	-	1.03	-	0	-	0.87	-
magistrale6	0	-	1.30	-	1	0.89	0.60	32.4%
outdoors5	1	16.52	14.87	10.0%	1	27.90	12.77	54.2%
outdoors7	1	7.93	7.59	4.2%	3	6.08	0.60	90.1%

Figure 7. The comparison of loop detection modules in terms of the number of detected loops, the estimated ATE with and without loop closure, as well as corresponding error reduction (rms ATE in meters). The results are the median of five executions. The ATE errors with loop closure are provided by Figure 6.

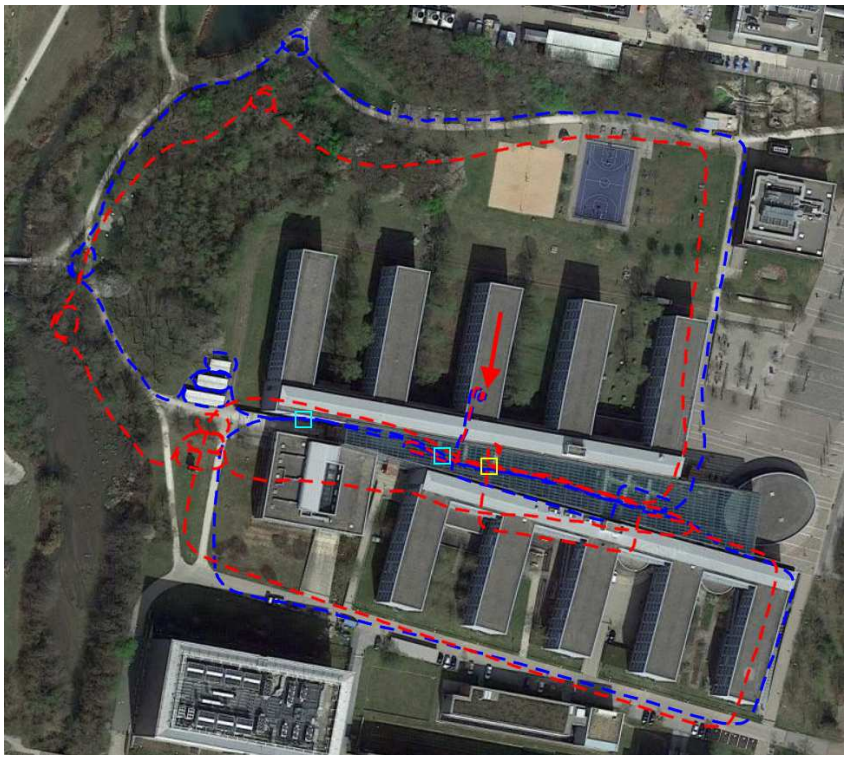

Figure 8. Estimated trajectories by HFNet-SLAM (blue) and ORB-SLAM3 (red) with the *outdoors7* sequence from TUM-VI dataset. Yellow squares denote the places for loop detection by both algorithms, while cyan squares denote the places for loop detection only by HFNet-SLAM. The red pointer points to the start and end of trajectories according to the ground truth data.

Secondly, the high quality of local features in HFNet-SLAM leads to accurate pose estimation. Figures 9 and 10 compare the performance of feature matching using ORB-SLAM3 and HFNet-SLAM in various environments during the evaluation. The matches with reprojection errors higher than 6 pixels are regarded as outliers. As can be seen, both algorithms have the highest matching precision in *room* sequences. However, as the environments get more complex, the precision significantly decreases in *magistrale* and *outdoors* sequences. In general, the tracking strategy of HFNet-SLAM tends to generate dense correspondences with high correctness in various environments. These results confirm the findings from both Sarlin et al. [16] and Tang et al. [32], which report that deep learning-based features have a higher matching score than hand-crafted algorithms. Excellent feature tracking provides sufficient and accurate pose estimation information and dramatically reduces the median ATE. This commonly occurs in some long sequences

without loop closure. Despite errors in the order of 10–42 m in these sequences, HFNet-SLAM still has the best accuracy in large environments.

Sequence	corridor	magistrale	outdoors	room	slides
ORB-SLAM3	61.3%	51.3%	61.8%	66.4%	62.1%
HFNet-SLAM	83.5%	78.7%	78.9%	85.9%	83.8%

Figure 9. Theaverage precision of feature matching in various environments.

There are also three *slides* sequences that contain tubular slides with dim lighting. These sequences are extremely different for feature-based SLAM systems to solve. HFNet-SLAM lost tracking in such dart slides because of the insufficient number of features for extracting and tracking, but it can solve the whole sequence based on the IMU measurements. The HFNet-SLAM has a better estimation of the inertial parameters, including gravity direction, IMU bias, and scale, which results in small ATEs in these sequences. Due to tracking failures in dark environments, it is recommended to use the optical flow or direct method to process featureless images.

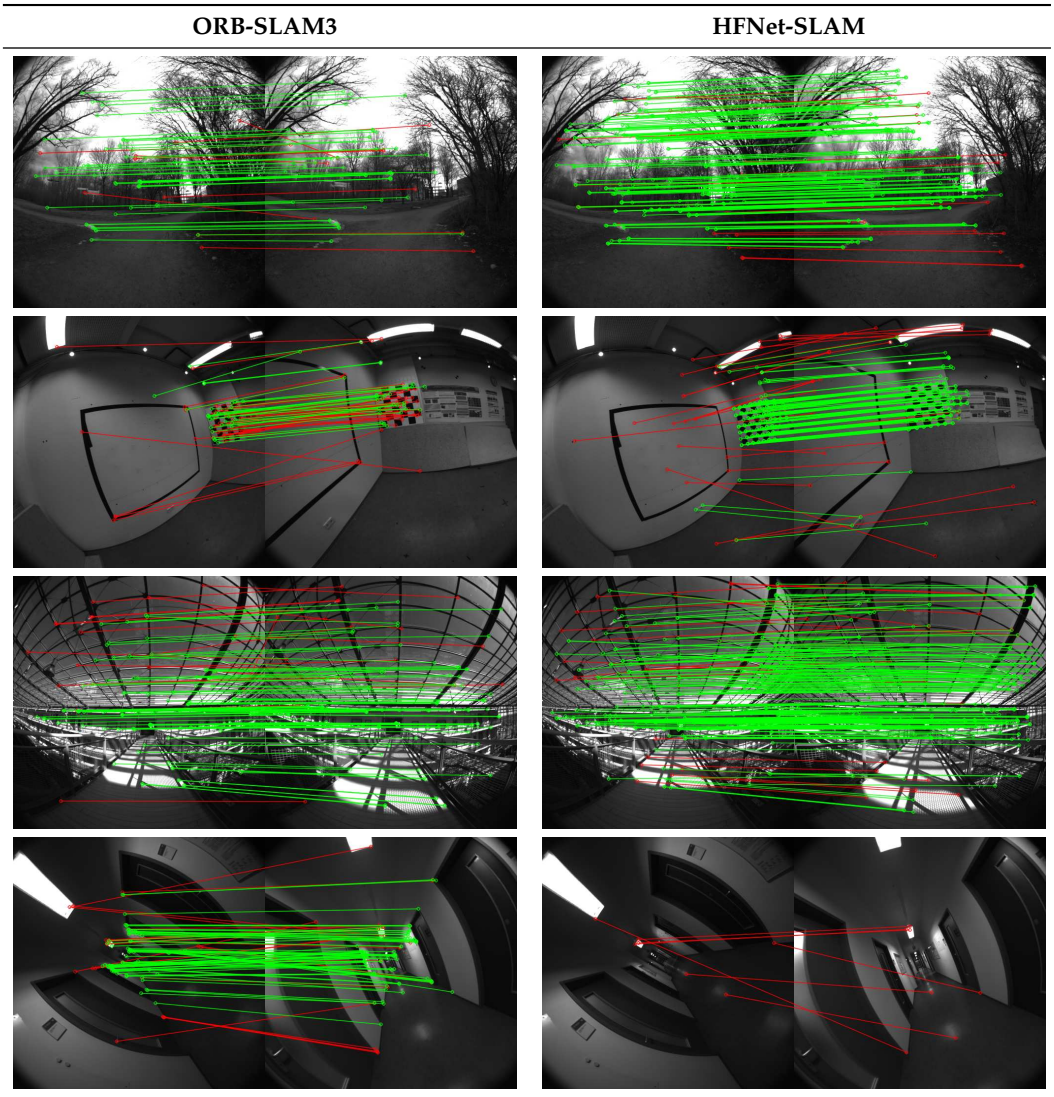

Figure 10. Qualitative results on feature matching. The green lines denote correct matches, while the red lines denote outliers. Row 4: Failure case due to extreme in-plane rotation.

One considerable disadvantage appears during the evaluation. As shown in Figure 10, HFNet-SLAM failed to find any correct matches due to the large in-plane rotation. Such extreme in-plane rotation can be seen in *corridor* sequences and corrupts the accuracy of the SLAM system. The key reason for this problem is that the SuperPoint encoder in HF-Net is not rotationally invariant due to insufficient related training examples [9].

To conclude, the introduction of HF-Net boosts the accuracy of tracking and loop detection, reducing the median ATE error compared with other state-of-the-art systems. However, the used model, HF-Net, has bad performance when input images are featureless or have a large in-plane rotation, which has a negative impact on the overall performance.

4.2. Runtime Performance

Figure 11 records the mean and standard deviation of the time consumption of the main parts of HFNet-SLAM while evaluating the EuRoC dataset. As the table shows, HFNet-SLAM performs the main operations in tracking, mapping, and loop closure threads, which are the same as ORB-SLAM3.

In the tracking thread, both ORB-SLAM3 and HFNet-SLAM take 10 milliseconds for feature extraction, which means that the inference of the HF-Net model optimised by TensorRT has a similar computational cost as the traditional ORB algorithm. In the mapping thread, compared with ORB-SLAM3, despite fewer features being extracted for every frame, the keypoint matching strategy in HFNet-SLAM provides a greater number of correct feature matches. As a result of that, the mapping thread can provide a comparable number of map points and information, which leads to a similar running time and map complexity. In the loop closure thread, the proposed loop detection module in HFNet-SLAM is effective in filtering the wrong loop in the database query stage, avoiding unnecessary calculation in the next geometric verification. Therefore, it is simpler and more efficient than the BoW-based method in ORB-SLAM3.

	System	ORB-SLAM3		HFNet-SLAM	
	Sensor	Monocular	Mono-Inertial	Monocular	Mono-Inertial
	CPU	Intel Core i7-10750H		Intel Core i7-10750H	
	GPU	-		NVIDIA RTX 2070 with Max-Q Design	
Settings	Resolution	752×480		752×480	
	Camera FPS	20Hz		20Hz	
	IMU Frequency	-	200Hz	-	200Hz
	Features Number	1000		675	
	Pyramid Levels	8		4	
	Feat. Extraction	10.35±1.88	10.38±1.88	10.07±0.97	10.16±1.04
	IMU Preintegration	-	0.10±0.06	-	0.09±0.05
Tracking	Pose Prediction	1.56±0.53	0.07±0.30	1.49±0.50	0.06±0.30
	LM Tracking	5.44±2.54	7.67±3.02	5.24±2.44	7.27±2.92
	Total	19.04±4.94	20.02±5.32	17.95±3.35	18.87±3.86
	KF Insertion	7.47±2.94	10.39±5.80	3.71±3.21	6.06±5.94
	MP Creation	24.21±11.48	31.99±15.17	25.59±15.77	34.37±17.60
Mapping	LBA	172.64±197.11	101.35±43.33	131.37±150.55	108.78±41.02
	KF Culling	20.62±17.49	25.10±20.07	19.24±17.82	27.09±23.73
	Total	223.73±220.60	169.16±85.74	179.10±180.35	178.03±94.47
	Database Query	0.48±0.27	0.62±0.26	0.27±0.17	0.33±0.16
Loop Detection	SE3 Estimation	3.65±3.32	3.26±2.27	0.10±1.93	0.21±3.06
	Total	4.13±3.57	2.85±2.69	0.41±1.93	0.49±2.77
Map Size	Key Frames	330	362	351	384
	Map Points	11733	11417	12452	13075

Figure 11. Processingtime of the main components of HFNet-SLAM compared with ORB-SLAM3, on EuRoC V202 (Time in millisecond).

In general, HFNet-SLAM is more effective than ORB-SLAM3 with the support of GPUs. This algorithm can run in real time at about 50 frames and 3-6 keyframes per second.

5. Conclusions and Future Work

Based on [1,16], this work proposes HFNet-SLAM, an accurate and real-time monocular SLAM system with deep features. The main contributions of this work, apart from the entire system itself, are the feature extraction strategy customized for deep CNNs as well as the keypoint matching and place recognition modules fully based on the generated local and global features. This work proves the practicality of incorporating deep features into the visual SLAM framework.

The experimental results showed that the appropriate application of deep features significantly improves the accuracy of pose estimation and loop detection and thereby boosts the accuracy of the entire HFNet-SLAM. The pure visual and visual-inertial configurations of HFNet-SLAM achieve the lowest errors, especially in complex and outdoor environments. Furthermore, with the support of GPU, SIMD, and TensorRT technology, HFNet-SLAM can run in real-time at 50 FPS.

There are two main disadvantages to HFNet-SLAM. The first one is the failure cases caused by the large in-plane rotation in camera motion because the used model, HF-Net, performs poorly with extreme rotation. Secondly, the calculation of this neural network needs the support of GPU accelerator resources, which may be impractical for mobile robot systems.

These drawbacks are the primary factors limiting the overall performance of the SLAM system. To address the problem, suggestions are given for future work. Firstly, when training neural networks for local feature extraction, it is reasonable to include more data with large in-plane rotation to improve rotation invariance. Secondly, some post-training optimisation tools, including quantization technology, can further reduce the cost of the HF-Net model, allowing the network to compute on CPUs. Last but not least, it is widely accepted that stereo and RGB-D SLAM have higher robustness and accuracy than the monocular configuration. Therefore, it is valuable to extend HFNet-SLAM to support different sensors.

Author Contributions: L.L. created the coding, performed experimentation and wrote the initial draft of the paper. J.M.A. provided supervision for the work, and has been involved during production of the paper. All authors have read and agreed to the published version of the manuscript.

Funding: This work is supported by the UK's Engineering and Physical Sciences Research Council (EPSRC) Programme Grant EP/S016813/1.

Institutional Review Board Statement: Not applicable.

Informed Consent Statement: Not applicable.

Data Availability Statement: The source code is available at: https://github.com/LiuLimingCode/HFNet_SLAM (accessed on 5 February 2023).

Conflicts of Interest: The authors declare no conflict of interest.

References

1. Campos, C.; Elvira, R.; Rodríguez, J.J.G.; Montiel, J.M.; Tardós, J.D. Orb-slam3: An accurate open-source library for visual, visual–inertial, and multimap slam. *IEEE Trans. Robot.* **2021**, *37*, 1874–1890.
2. Qin, T.; Li, P.; Shen, S. Vins-mono: A robust and versatile monocular visual-inertial state estimator. *IEEE Trans. Robot.* **2018**, *34*, 1004–1020.
3. Leutenegger, S.; Lynen, S.; Bosse, M.; Siegwart, R.; Furgale, P. Keyframe-based visual–inertial odometry using nonlinear optimization. *Int. J. Robot. Res.* **2015**, *34*, 314–334.
4. Bujanca, M.; Shi, X.; Spear, M.; Zhao, P.; Lennox, B.; Luján, M. Robust SLAM Systems: Are We There Yet? In Proceedings of the 2021 IEEE/RSJ International Conference on Intelligent Robots and Systems (IROS), Prague, Czech Republic, 27 September–1 October 2021; pp. 5320–5327.
5. Evans, M.H.; Aitken, J.M.; Anderson, S.R. Assessing the feasibility of monocular visual simultaneous localization and mapping for live sewer pipes: A field robotics study. In Proceedings of the 2021 IEEE 20th International Conference on Advanced Robotics (ICAR), Ljubljana, Slovenia, 6–10 December 2021; pp. 1073–1078.
6. Aitken, J.M.; Evans, M.H.; Worley, R.; Edwards, S.; Zhang, R.; Dodd, T.; Mihaylova, L.; Anderson, S.R. Simultaneous localization and mapping for inspection robots in water and sewer pipe networks: A review. *IEEE Access* **2021**, *9*, 140173–140198.

7. Macario Barros, A.; Michel, M.; Moline, Y.; Corre, G.; Carrel, F. A comprehensive survey of visual slam algorithms. *Robotics* **2022**, *11*, 24.
8. Yi, K.M.; Trulls, E.; Lepetit, V.; Fua, P. Lift: Learned invariant feature transform. In Proceedings of the European Conference on Computer Vision, Amsterdam, The Netherlands, 11–14 October 2016; Springer: Berlin/Heidelberg, Germany, 2016; pp. 467–483.
9. DeTone, D.; Malisiewicz, T.; Rabinovich, A. Superpoint: Self-supervised interest point detection and description. In Proceedings of the IEEE Conference on Computer Vision and Pattern Recognition Workshops, Salt Lake City, UT, USA, 18–22 June 2018; pp. 224–236.
10. Schonberger, J.L.; Hardmeier, H.; Sattler, T.; Pollefeys, M. Comparative evaluation of hand-crafted and learned local features. In Proceedings of the IEEE Conference on Computer Vision and Pattern Recognition, Honolulu, HI, USA, 21–26 July 2017; pp. 1482–1491.
11. Ma, J.; Jiang, X.; Fan, A.; Jiang, J.; Yan, J. Image matching from handcrafted to deep features: A survey. *Int. J. Comput. Vis.* **2021**, *129*, 23–79.
12. Gálvez-López, D.; Tardos, J.D. Bags of binary words for fast place recognition in image sequences. *IEEE Trans. Robot.* **2012**, *28*, 1188–1197.
13. Arshad, S.; Kim, G.W. Role of deep learning in loop closure detection for visual and lidar slam: A survey. *Sensors* **2021**, *21*, 1243.
14. Memon, A.R.; Wang, H.; Hussain, A. Loop closure detection using supervised and unsupervised deep neural networks for monocular SLAM systems. *Robot. Auton. Syst.* **2020**, *126*, 103470.
15. Merrill, N.; Huang, G. Lightweight unsupervised deep loop closure. *arXiv* **2018**, arXiv:1805.07703.
16. Sarlin, P.E.; Cadena, C.; Siegwart, R.; Dymczyk, M. From coarse to fine: Robust hierarchical localization at large scale. In Proceedings of the IEEE/CVF Conference on Computer Vision and Pattern Recognition, Long Beach, CA, USA, 15–20 June 2019; pp. 12716–12725.
17. Davison, A.J. Real-time simultaneous localisation and mapping with a single camera. In Proceedings of the Computer Vision, IEEE International Conference on. IEEE Computer Society, Nice, France, 13–16 October 2003; Volume 3, p. 1403.
18. Mourikis, A.I.; Roumeliotis, S.I. A Multi-State Constraint Kalman Filter for Vision-aided Inertial Navigation. In Proceedings of the 2007 IEEE International Conference on Robotics and Automation, Rome, Italy, 10–14 April 2007; Volume 2, p. 6.
19. Chen, Y.; Chen, Y.; Wang, G. Bundle adjustment revisited. *arXiv* **2019**, arXiv:1912.03858.
20. Li, R.; Wang, S.; Long, Z.; Gu, D. Undeepvo: Monocular visual odometry through unsupervised deep learning. In Proceedings of the 2018 IEEE International Conference on Robotics and Automation (ICRA), Brisbane, Australia, 21–25 May 2018; pp. 7286–7291.
21. Wang, S.; Clark, R.; Wen, H.; Trigoni, N. Deepvo: Towards end-to-end visual odometry with deep recurrent convolutional neural networks. In Proceedings of the 2017 IEEE International Conference on Robotics and Automation (ICRA), Singapore, 29 May–3 June 2017; pp. 2043–2050.
22. Li, R.; Wang, S.; Gu, D. Deepslam: A robust monocular slam system with unsupervised deep learning. *IEEE Trans. Ind. Electron.* **2020**, *68*, 3577–3587.
23. Liu, Y.; Miura, J. RDS-SLAM: Real-time dynamic SLAM using semantic segmentation methods. *IEEE Access* **2021**, *9*, 23772–23785.
24. Zhao, C.; Sun, Q.; Zhang, C.; Tang, Y.; Qian, F. Monocular depth estimation based on deep learning: An overview. *Sci. China Technol. Sci.* **2020**, *63*, 1612–1627.
25. Rublee, E.; Rabaud, V.; Konolige, K.; Bradski, G. ORB: An efficient alternative to SIFT or SURF. In Proceedings of the 2011 IEEE International Conference on Computer Vision, Barcelona, Spain, 6–13 November 2011; pp. 2564–2571.
26. Shi, J. Good features to track. In Proceedings of the 1994 IEEE Conference on Computer Vision and Pattern Recognition, Seattle, WA, USA, 21–23 June 1994; pp. 593–600.
27. Leutenegger, S.; Chli, M.; Siegwart, R.Y. BRISK: Binary robust invariant scalable keypoints. In Proceedings of the 2011 IEEE International Conference on Computer Vision, Barcelona, Spain, 6–13 November 2011; pp. 2548–2555.
28. Revaud, J.; Weinzaepfel, P.; De Souza, C.; Pion, N.; Csurka, G.; Cabon, Y.; Humenberger, M. R2D2: Repeatable and reliable detector and descriptor. *arXiv* **2019**, arXiv:1906.06195.
29. Dusmanu, M.; Rocco, I.; Pajdla, T.; Pollefeys, M.; Sivic, J.; Torii, A.; Sattler, T. D2-net: A trainable cnn for joint description and detection of local features. In Proceedings of the IEEE/CVF Conference on Computer Vision and Pattern Recognition, Long Beach, CA, USA, 15–20 June 2019; pp. 8092–8101.
30. Tyszkiewicz, M.; Fua, P.; Trulls, E. DISK: Learning local features with policy gradient. *Adv. Neural Inf. Process. Syst.* **2020**, *33*, 14254–14265.
31. Ono, Y.; Trulls, E.; Fua, P.; Yi, K.M. LF-Net: Learning local features from images. In Proceedings of the Advances in Neural Information Processing Systems, Montreal, QC, Canada, 3–8 December 2018; Volume 31.
32. Tang, J.; Ericson, L.; Folkesson, J.; Jensfelt, P. GCNv2: Efficient correspondence prediction for real-time SLAM. *IEEE Robot. Autom. Lett.* **2019**, *4*, 3505–3512.
33. Kang, R.; Shi, J.; Li, X.; Liu, Y.; Liu, X. DF-SLAM: A deep-learning enhanced visual SLAM system based on deep local features. *arXiv* **2019**, arXiv:1901.07223.
34. Nister, D.; Stewenius, H. Scalable recognition with a vocabulary tree. In Proceedings of the 2006 IEEE Computer Society Conference on Computer Vision and Pattern Recognition (CVPR'06), New York, NY, USA, 17–22 June 2006; Volume 2, pp. 2161–2168.
35. Garcia-Fidalgo, E.; Ortiz, A. ibow-lcd: An appearance-based loop-closure detection approach using incremental bags of binary words. *IEEE Robot. Autom. Lett.* **2018**, *3*, 3051–3057.

36. Zhang, X.; Su, Y.; Zhu, X. Loop closure detection for visual SLAM systems using convolutional neural network. In Proceedings of the 2017 IEEE 23rd International Conference on Automation and Computing (ICAC), Huddersfield, UK, 7–8 September 2017; pp. 1–6.
37. Arandjelovic, R.; Gronat, P.; Torii, A.; Pajdla, T.; Sivic, J. NetVLAD: CNN architecture for weakly supervised place recognition. In Proceedings of the IEEE Conference on Computer Vision and Pattern Recognition, Las Vegas, NV, USA, 27–30 June 2016; pp. 5297–5307.
38. Hausler, S.; Garg, S.; Xu, M.; Milford, M.; Fischer, T. Patch-netvlad: Multi-scale fusion of locally-global descriptors for place recognition. In Proceedings of the IEEE/CVF Conference on Computer Vision and Pattern Recognition, Nashville, TN, USA, 19–25 June 2021; pp. 14141–14152.
39. Yang, Y.; Tang, D.; Wang, D.; Song, W.; Wang, J.; Fu, M. Multi-camera visual SLAM for off-road navigation. *Robot. Auton. Syst.* **2020**, *128*, 103505.
40. Kuse, M.; Shen, S. Learning whole-image descriptors for real-time loop detection and kidnap recovery under large viewpoint difference. *Robot. Auton. Syst.* **2021**, *143*, 103813.
41. Cao, B.; Araujo, A.; Sim, J. Unifying deep local and global features for image search. In Proceedings of the European Conference on Computer Vision, Glasgow, UK, 23–28 August 2020; Springer: Berlin/Heidelberg, Germany, 2020; pp. 726–743.
42. Sandler, M.; Howard, A.; Zhu, M.; Zhmoginov, A.; Chen, L.C. Mobilenetv2: Inverted residuals and linear bottlenecks. In Proceedings of the IEEE Conference on Computer Vision and Pattern Recognition, Salt Lake City, UT, USA, 18–23 June 2018; pp. 4510–4520.
43. Li, D.; Shi, X.; Long, Q.; Liu, S.; Yang, W.; Wang, F.; Wei, Q.; Qiao, F. DXSLAM: A robust and efficient visual SLAM system with deep features. In Proceedings of the 2020 IEEE/RSJ International Conference on Intelligent Robots and Systems (IROS), Las Vegas, NV, USA, 24 October 2020–24 January 2021; pp. 4958–4965.
44. Jeong, E.; Kim, J.; Tan, S.; Lee, J.; Ha, S. Deep learning inference parallelization on heterogeneous processors with tensorrt. *IEEE Embed. Syst. Lett.* **2021**, *14*, 15–18.
45. Flynn, M.J. Some computer organizations and their effectiveness. *IEEE Trans. Comput.* **1972**, *100*, 948–960.
46. Fischler, M.A.; Bolles, R.C. Random sample consensus: A paradigm for model fitting with applications to image analysis and automated cartography. *Commun. ACM* **1981**, *24*, 381–395.
47. Burri, M.; Nikolic, J.; Gohl, P.; Schneider, T.; Rehder, J.; Omari, S.; Achtelik, M.W.; Siegwart, R. The EuRoC micro aerial vehicle datasets. *Int. J. Robot. Res.* **2016**, *35*, 1157–1163.
48. Schubert, D.; Goll, T.; Demmel, N.; Usenko, V.; Stückler, J.; Cremers, D. The TUM VI benchmark for evaluating visual-inertial odometry. In Proceedings of the 2018 IEEE/RSJ International Conference on Intelligent Robots and Systems (IROS), Madrid, Spain, 1–5 October 2018; pp. 1680–1687.
49. Sturm, J.; Engelhard, N.; Endres, F.; Burgard, W.; Cremers, D. A benchmark for the evaluation of RGB-D SLAM systems. In Proceedings of the 2012 IEEE/RSJ international conference on intelligent robots and systems, Vilamoura-Algarve, Portugal, 7–12 October 2012; pp. 573–580.
50. Zubizarreta, J.; Aguinaga, I.; Montiel, J.M.M. Direct sparse mapping. *IEEE Trans. Robot.* **2020**, *36*, 1363–1370.